Materials Advances

ROYAL SOCIETY OF CHEMISTRY

PAPER

View Article Online
View Journal | View Issue

Cite this: *Mater. Adv.*, 2025, 6, 3523

Effects of the shear rate on dispersion characteristics of industrial-based functionalized/non functionalized graphene in an epoxy matrix†

Sabyasachi Ghosh, *[a] Jitendra Bhatia,[a] Amit Gupta,[a] Chandrani Pramanik, *[b] Sumit Pratihar[b] and Debabrata Rautaray[a]

Epoxy resin, widely recognized for its durability and chemical resistance, exhibits superior performance when reinforced with nanofillers, making it ideal for demanding engineering applications. This research aims to explore the state-of-the-art developments in epoxy resin and graphene composites *via* two industrially feasible approaches, such as mechanical stirring (MS) and a high-speed shearing process (HSS), providing insights into the mechanisms of reinforcement and the resulting improvements in material characteristics. As nano-additives, two varieties of graphene powders—functionalized (Gp-C) and non-functionalized (Gp-A)—are chosen. On fractured surfaces, XRD measurements and electron microscopy (both FESEM and HRTEM) are used to verify the filler dispersion and the creation of a strong interface within the epoxy matrix. The remaining functional groups in Gp-C have the ability to react with anhydride or epoxy groups to produce covalent bonds that improve the mechanical and thermal properties of the composite by improving interfacial adhesion. On the other hand, Gp-A graphene reduces the composite's overall mechanical properties by producing an uneven dispersion and possible weak spots. We expanded the research by utilizing Gp-A and Gp-C graphenes (tensile strength of 380 ± 20 MPa, around 10% and 420 ± 20 MPa, about 22% improvements) as fillers in glass fiber single-layer epoxy laminates, building on the incorporation of graphene fillers in epoxy resin. The goal was to examine not only the mechanical enhancements but also the antibacterial properties (zone of inhibition (ZOI) values of 1.2 mm^2 for *E. coli* and 1.8 mm^2 for *S. aureus* in the GNF (Gp-A) laminate and 0.8 mm^2 for both bacteria in the GF (Gp-C) laminate). The antibacterial efficacy of graphene-coated epoxy laminates was evaluated using CFU (colony-forming unit) testing, where GNF achieved a log reduction of ≥1.61 for *E. coli* and 0.49 for *S. aureus*, while GF demonstrated enhanced antibacterial activity with log reductions of 1.13 for *E. coli* and 3.38 for *S. aureus*, attributed to ROS-mediated oxidative stress and bacterial membrane disruption. This study addresses the challenges in dispersing nano-additives in epoxy resin and highlights innovative industrial development prospects, offering valuable insights for enhancing performance in demanding engineering sectors, including infrastructure, marine, and chemical processing industries.

Received 24th February 2025,
Accepted 13th April 2025

DOI: 10.1039/d5ma00173k

rsc.li/materials-advances

1. Introduction

Epoxy resin is a versatile and widely used thermosetting polymer that has gained significant attention in composite material applications due to its exceptional mechanical properties, adhesion, and durability.[1–3] However, epoxy resins are known for their rigidity and brittleness due to their crosslinked structures, which can limit their suitability in applications requiring resistance to crack initiation and propagation, such as structural materials for high-load applications.[4,5] Composite materials, composed of a reinforcing phase embedded in a matrix, have gained prominence for their ability to synergistically combine the unique properties of different materials, resulting in enhanced performance and tailored functionalities.[6–8] When reinforced with fibers such as glass/carbon, or synthetic ceramics, epoxy-based composites exhibit exceptional strength-to-weight ratios, making them invaluable in industries ranging from aerospace to automotive.[9–12] Additionally, resins exhibit minimal shrinkage and emit fewer toxic substances during the

[a] *DCM Shriram Innovation Centre, DCM Shriram Limited, Gujarat 391410, India. E-mail: sabyasachighosh@dcmshriram.com*
[b] *Graphene Centre, Tata Steel Limited, Jamshedpur 831007, India. E-mail: chandrani.pramanik@tatasteel.com*

† Electronic supplementary information (ESI) available. See DOI: https://doi.org/10.1039/d5ma00173k

curing process.[13] As a result, epoxy resin-based composites are regarded as premium materials widely used on an industrial scale, despite their high cost.[14]

However, to further elevate the performance of these composites, industrial researchers are turning to functionalized graphene as a reinforcing agent. The tribological properties of resins can indirectly affect their mechanical strength, although epoxy resins typically exhibit limited tribological capabilities.[15,16] A material's toughness, or its ability to absorb mechanical impact, necessitates high force resistance and deformation mechanisms that absorb and dissipate applied mechanical energy over a substantial path, large volume, and extended time.[17,18] These mechanisms may be inherent to the material's microstructure or intentionally incorporated into the structure of polymer/epoxy resin composites and blends.[19,20] To enhance mechanical and thermal properties, epoxy composites reinforced or toughened with nanomaterials have attracted significant interest from both academic and industrial circles. Achieving a synergistic effect requires the careful selection of micro and nanosized filler additives (such as graphene nanoplatelets (GnPs), carbon nanotubes (CNTs), halloysite nanotubes (HNTs), carbon blacks, *etc.*), along with considerations of shape, surface chemistry, and the modulation of the matrix's physicochemical characteristics.[21–24] Achieving superior strength in epoxies through the addition of nanoparticles relies on various factors: (i) obtaining the right nanoparticle concentration, (ii) prevention of agglomerates through effective mixing techniques, (iii) ensuring robust filler adhesion, and (iv) promoting chemical interaction with the matrix. To effectively harness these enhancements, a comprehensive understanding of how these additives influence structure formation processes and the resulting composite structure is essential.

Graphene, renowned as the world's first 2D material, has captivated researchers with its exceptional electronic, mechanical, and chemical properties.[25,26] Despite its promise, graphene's high specific surface area leads to the formation of irreversible agglomerates or restacking due to van der Waals interactions and π–π stacking. Typically, graphene sheets are randomly dispersed in epoxy resins, preventing the full utilization of graphene's anisotropic properties inherent in its laminated structure. To mitigate this issue, a highly effective approach involves the chemical exfoliation of graphite into graphene, and subsequently into functionalized graphene.[27] Incorporating the oxidized form of graphene into a polymer matrix enhances the versatility of interactions, thanks to the presence of oxygen-containing polar functionalities such as carboxyl, carbonyl, epoxide, and hydroxyl groups.[28] The combined effect of any coupling agent, such as silane and an epoxy or a polyurethane matrix, significantly improved the adhesion characteristics of the aluminum alloy coating. A 50% graphene oxide–silane/epoxy/2% graphene oxide–polyurethane system exhibited superior performance with a 9068% increase in real impedance, while a 50% graphene oxide–silane/epoxy system exhibited a 759% improvement, both with minimal coating removal (5%) in adhesion tests. These results confirm the effective integration of functionalized graphene oxide for long-term metal protection, offering an eco-friendly, mechanically robust, and high-performance anti-corrosion solution for aerospace applications.[29,30] Furthermore, to unambiguously determine how graphene and its functionalization affect the mixing behaviour of epoxy using various industrially viable techniques, it requires that the complicated interaction between the filler/matrix epoxy should be clarified and understood. Physical stirring (*i.e.*, high-speed shearing and mechanical stirring) in a polymer matrix is a more industrially viable method than chemical exfoliation due to its simplicity, cost-effectiveness, and scalability. Unlike chemical exfoliation, which involves complex processes and environmental concerns, physical mixing efficiently disperses fillers without requiring hazardous chemicals, making it ideal for large-scale production.

In this work, we explore the synergistic potential of combining epoxy resin with both functionalized graphene (*e.g.*, Gp-C named as GF) and non-functionalized graphene (*e.g.*, Gp-A named as GNF), with a focus on achieving superior mechanical and thermal characteristics in epoxy-based composites. The main objective here is to elucidate the industrially viable mixing behaviour of nano-additives and the dispersion mechanisms within these composites. A special emphasis is placed on observing how the functionalization of graphene interacts with the epoxy curing process. The incorporation of very minimal doses of functionalized graphene opens up avenues for achieving improved structural integrity in structural composite applications. This study examines methods to effectively balance thermal and mechanical properties in epoxy castings. In contrast to the earlier observations, we expanded the scope to fabricate single-layer glass fabric laminates incorporating an epoxy/graphene system, aimed at developing high-performance fiber-reinforced polymers (FRPs) with enhanced mechanical properties. Additionally, the system was applied to create stable coating solutions for top-coated FRPs, offering antibacterial protection for applications such as FRP composite pipes in water treatment, medical devices, and filtration systems. The findings highlight the potential for significantly enhancing the performance of composite materials, rendering them suitable for advanced engineering applications.

2. Experimental

2.1. Raw materials

A modified DGEBA-based epoxy system containing a reactive diluent, a carboxylic anhydride hardener, and an amine-based accelerator was obtained from the local chemical market of Vadodara, Gujarat. Gp-C (functionalized graphene, GF $\leq$ 20 layers, bulk density: 0.3–0.4 g cm^{-3}, lateral dimension: 5 $\pm$ 2 μm, C ~80–89%, N ~0.2–0.4%, H ~1–1.3%, S ~0.036–0.15%) and Gp-A (non functionalized graphene, GNF ~20 layers, bulk density: 0.01–0.02 g cm^{-3}, lateral dimension: 10 $\pm$ 7 μm, C ~93–94%, S ~0.2–0.3%, H ~0.1–0.2%) graphene samples were acquired from Graphene Centre, Tata Steel Ltd. 610 BD (Bi-Directional) woven Glass Fabric of 610 GSM was collected from a local market, Vadodara, India.

2.2. Fabrication of functionalized (F) and non-functionalized (NF) graphene-embedded epoxy composites applying high-speed shearing (HSS) and mechanical stirring (MS) processes

A calculated quantity of both NF/F-graphene (0.1 wt%) was evenly dispersed in a solution of epoxy resin and a diluent. Two distinct methods were employed for thorough mixing: (i) high-speed mixer grinding at approximately ∼18 000 rpm and (ii) mechanical stirring at around 1000 rpm. Subsequently, the hardener was introduced to the solution, and the mixture underwent an additional 1 minute of stirring (for mixer grinding) and 1 hour of stirring (for mechanical stirring) to ensure proper dispersion and achieve a homogeneous distribution of graphene batches within the epoxy matrix. Following this step, the solutions were placed in a vacuum oven at 27 °C (and 5 bar pressure) for 20 min and subjected to degassing to eliminate any entrapped air within the epoxy/graphene system. Finally, the solution was molded at 80 °C for 6 hours, followed by post-curing at 130 °C for 6 hours, and a detailed schematic presentation is provided in Fig. 1.

3. Characterization

The morphological characteristics of the epoxy/f-graphene composites were investigated by field emission-scanning electron microscopy (SEM) with a thin layer of Au and at a 5 kV acceleration voltage for 2 min. High-resolution transmission electron microscopy (HRTEM, JEM-2100, 200 kV, Tokyo, Japan) was also employed, with ultrathin sections prepared using a Leica Ultra Cut UCT ultramicrotome (Leica Microsystems, Vienna, Austria). To assess the mechanical properties, both the untreated epoxy and the epoxy composites containing f-graphene were tested using a universal testing machine (UTM, Instron, High Wycombe, England at 100 kN load). Tensile tests were conducted with a crosshead speed of 10 mm min^{-1}, while flexural measurements were performed at a speed of 1.5 mm min^{-1}. Thermal durability was assessed using a thermogravimetric analyzer (TGA, Parkin Elmer, TEAN 5320020, USA) at a heating rate of 10 °C min^{-1} in an inert nitrogen environment, over a temperature range of 50 to 1100 °C. The antibacterial tests of the top-coated laminates were performed by inhibition zone measurement in the Mueller–Hinton agar plate (incubation conditions: 37 ± 1 °C for 24 h and replicates: n = 1). *Escherichia coli* (*E. coli*, ATCC 10536, gram −ve) and *Staphylococcus aureus* (*S. aureus*, ATCC 6538, gram +ve) bacteria were used as models for antibacterial measurement. Moreover, ISO 22196 is used to measure the antibacterial activity of non-porous surfaces by incubating bacteria (*e.g.*, *E. coli* and *S. aureus*) on the coated laminates and assessing their reduction after 24 hours, and quantified as a log reduction value.

4. Results and discussion

To fully utilize the outstanding performance of graphene fillers in an epoxy matrix, it is essential to achieve adequate exfoliation and effective dispersion of fillers within the matrix. Fig. 2(A and B) shows the fractured surfaces of the epoxy composites. After incorporation with graphene nanoflakes, the changes in the matrix phase (epoxy) were observed. Micrographs for the GF/epoxy nanocomposites (MS) show homogeneously distributed aggregates due to a favourable graphene interaction with the epoxy matrix, whereas GNF/epoxy nanocomposites (MS) show loosely packed isolated aggregates of graphene nanoplatelets (Fig. 2(C and D)). Such aggregates form due to graphene's unfavourable interactions with the epoxy matrix and strong *van der Waals* attraction forces with nanoplatelets.[31] The bonding between the hydroxyl, epoxide, and anhydride groups of the cured ER resin and the hydroxyl groups on the surface of GF graphene involves hydrogen bonding. Additionally, there might be an OH–π interaction playing a role between the benzene ring of the ER resin and the hydroxyl groups of the functionalized

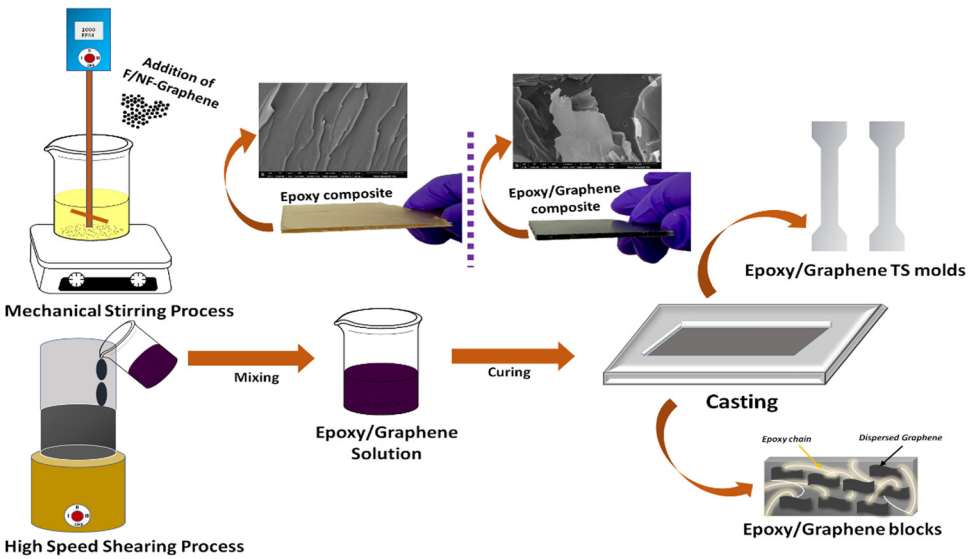

Fig. 1 Schematic of the preparation of epoxy/graphene composites *via* different stirring processes.

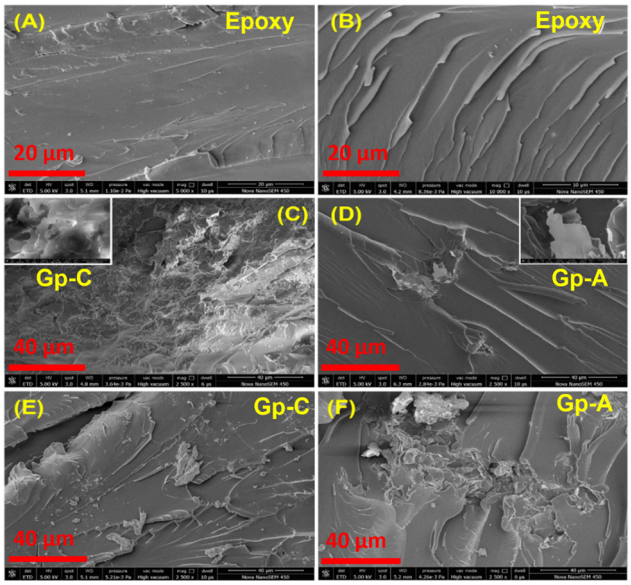

Fig. 2 FESEM micrographs of (A) and (B) fractured epoxy composites; (C) and (D) functionalized graphene/epoxy and non-functionalized graphene/epoxy nanocomposites *via* mechanical stirring; (E) and (F) functionalized graphene/epoxy and non-functionalized graphene/epoxy nanocomposites *via* high-speed shearing.

graphene surface.[32] These interactions, particularly the hydrogen bonding, exhibit substantial orbital interaction energy, thus playing a significant role in enhancing adhesive strength (*i.e.*, reinforcing) at the epoxy/functionalized (GF) graphene interface, consequently contributing to the superior mechanical properties observed.[33] During HSS, the micrographs for both GF/epoxy nanocomposites and GNF/epoxy nanocomposites showed loosely packed isolated aggregates. Due to the sharp blades and high-speed mixing, a few aggregates lowered down in size, and some of them are high, which relate to the inhomogeneous distribution (Fig. 2(E and F)). Additional characterization by elemental mapping *via* energy-dispersive X-ray spectroscopy (EDX) was carried out, which clearly differentiates the well-dispersed from the not-so-well-dispersed samples that have been developed by incorporating the graphene fillers (both functionalized and non-functionalized) in the epoxy matrix. Moreover, the dispersion is quite visible under light through digital photographs for both functionalized and non-functionalized graphene (Fig. S1, ESI†).

In the XRD micrographs (shown in Fig. 3), GNF/epoxy composites showed two peaks at 26° and 29°, which are linked to the layered crystalline graphene platelets, signifying that the layered structure is retained in each platelet. Conversely, a broad peak at 13° corresponds to the pure epoxy amorphous zone. However, GF/epoxy composites show no distinct diffraction peaks, displaying only an amorphous region at 13.2° and a slightly broad peak at 25° due to the exfoliation of graphene platelets, mostly related to reduced graphene oxide.[34]

In the FTIR spectra, a peak at 1729 cm^{-1} is associated with the stretching vibration of C═O in a non-conjugated ester, whereas those at 2914–2955 cm^{-1} are associated with the –C–H stretching vibration of methyl and methylene groups (epoxy) and peak intensity slightly changes after addition of graphene in the epoxy matrix.[35] Peaks at 1606–1459 cm^{-1} are associated with the C═C aromatic vibration related to π–π interactions with epoxy and graphene. Peaks at 687–624 cm^{-1} signify the aromatic structure,[36] which is intact after the addition of both functionalized/non-functionalized graphene. In functionalized graphene/epoxy composites, one additional broad peak was observed at 3622 cm^{-1} related to the inter-molecular hydrogen bonding with the hydroxyl (–OH) functional group[37] (Fig. S2, ESI†).

Fig. 4 illustrates the mechanical properties of the GNF and GF/epoxy composites. The tensile and flexural strength, as well as the modulus of the two different mixing techniques, exhibit various characteristics. For the high shear mixing (HSS) technique, composites with GF show a 1% increase in flexural strength, while those with GNF show a 30% decrease. The tensile strength and modulus for the GF composites decrease by 20% and 6%, respectively. In contrast, the GNF composites exhibit a 24% decrease in tensile strength and a 4% increase in modulus compared to pristine epoxy. Using the mechanical stirring (MS) technique, composites with GF demonstrate a 19% increase in flexural strength, while those with GNF show a 12% decrease. The tensile strength and modulus for the GF composites increase by 18% and decrease by 3%, respectively. In comparison, the GNF composites exhibit a 15% decrease in tensile strength and a 0.5% decrease in modulus compared to pristine epoxy. Comparatively, using the HSS method,

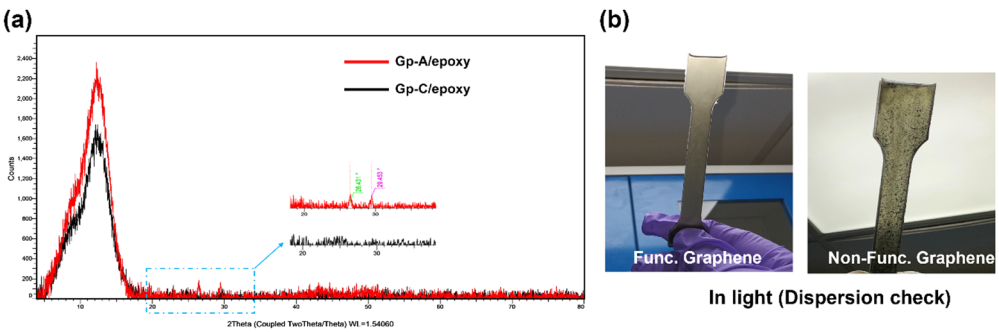

Fig. 3 (a) XRD micrographs of Gp-A/epoxy and Gp-C/epoxy composites; (b) digital photograph for in-light dispersion visualization of GF/epoxy (mostly homogeneous) and GNF/epoxy composites (agglomerated and not consistent).

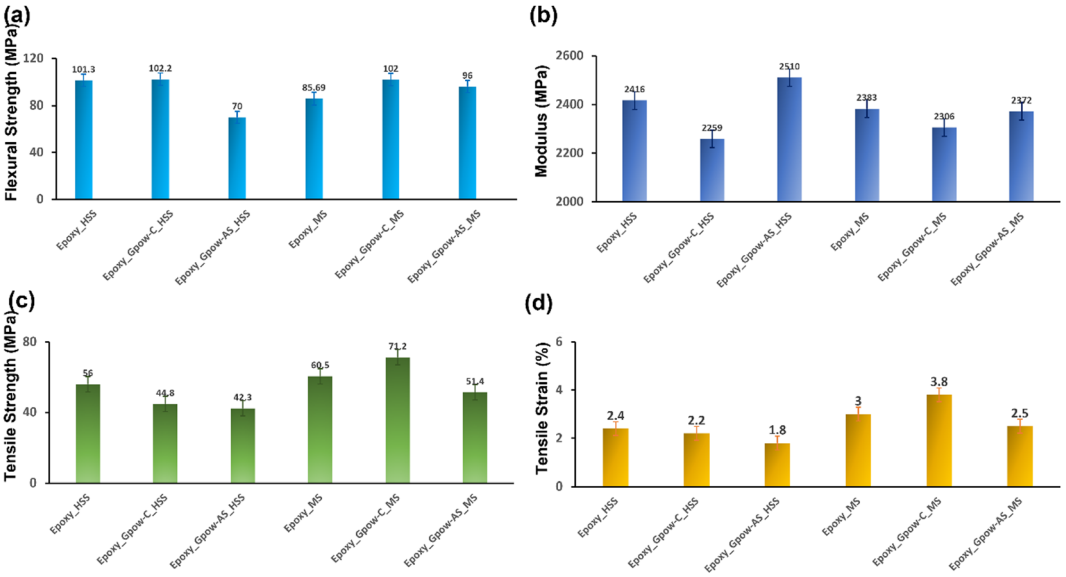

Fig. 4 Mechanical characteristics (a) flexural strength (MPa), (b) modulus (MPa), (c) tensile strength (MPa), and (d) tensile strain (%) of epoxy, GF and GNF-based composites with the variation of high-speed shearing (HSS) and mechanical stirring (MS); (three samples were tested and taking the average for each method).

GF-loaded composites maintain flexural strength, but their tensile properties decline to some extent. The GNF-loaded composites experience significant drops in all mechanical characteristics, highlighting the importance of functionalization. Additionally, the HSS process is not as effective as initially assumed, despite expectations that high-speed (~18 000 rpm) graphene particles would produce a homogeneous mixture. Mechanical stirring likely ensures a more even distribution of the hardener in epoxy, improving crosslinking and slightly enhancing tensile strength and strain. In contrast, high-speed shearing may lead to over-mixing, introducing air bubbles, or generating more heat, which might accelerate the curing process unevenly or cause local hotspots, leading to inconsistencies in the cured matrix, ultimately reducing tensile strength. This uniformity enhances the material's ability to resist bending forces, which explains the opposite trend for the flexural properties.

GNF-based non-functionalized graphene tends to agglomerate in epoxy composites, making it easy for cracks to initiate and propagate, thereby reducing the overall strength of the composites.[38] In contrast, GF displays dispersed graphene fillers (see Fig. 2C and D) that transfer applied loads more efficiently than the aggregated fillers. However, the high shear mixing (HSS) process can eventually break the graphene structure into both functionalized and non-functionalized forms, leading to degraded mechanical performance. A strong interfacial bond between the graphene sheets and the epoxy matrix is crucial for determining the properties of polymer composites. GF sheets provide a strong interface due to homogeneous mixing, allowing effective load transfer from the epoxy to the sheets, which may break under high loading.[39] The additional nitrogen element introduced during functionalization interferes with the curing process of the epoxy system and anhydride hardener, either directly participating in the reaction or acting as a catalyst, enhancing overall cross-linking and thereby improving the mechanical and thermal properties of the final cured GF/epoxy composites.[40] GNF has a balanced number of defects and functional groups that can help in stress dissipation and load transfer. GNF, with its fewer defects, might not distribute stress as effectively, leading to lower overall strength in the composite. The plausible interaction phenomena are shown in Fig. 5.

In addition, residual functional groups of GF can react with epoxy or anhydride groups, forming covalent bonds that enhance the interfacial adhesion and improve the mechanical properties of the composite. In contrast, GNF leads to uneven dispersion and potential weak points in the composite, diminishing its overall strength and mechanical properties.

HRTEM imaging was conducted to further examine the structural characteristics of composites incorporating GNF and GF additives, as shown in Fig. 6. The selected area electron diffraction (SAED) pattern reveals diffraction spots, indicating the crystalline nature of GNF. The observed fringes show a lattice constant of 0.235 nm, which is close to the 0.246 nm lattice parameter of graphene's triangular lattice structure.[41] In the GF blended epoxies, aggregated graphene flakes exhibit an interlayer spacing of 0.339 nm, which is higher than that of graphite (0.337 nm), suggesting an increase in the interlayer spacing due to functionalization (involvement of functional groups). However, SAED indicates that the lattice order across the flakes is poor (lower crystallinity due to functionalization) compared to the high crystallinity observed in GNF/epoxy because of its π–π stacking feature, owing to non-functional character, and stacking energy is favorable to the epoxy–graphene layers.

Thermal gravimetric analysis (TGA) was conducted on pure epoxy and a composite of graphene/epoxy (GF & GNF) to

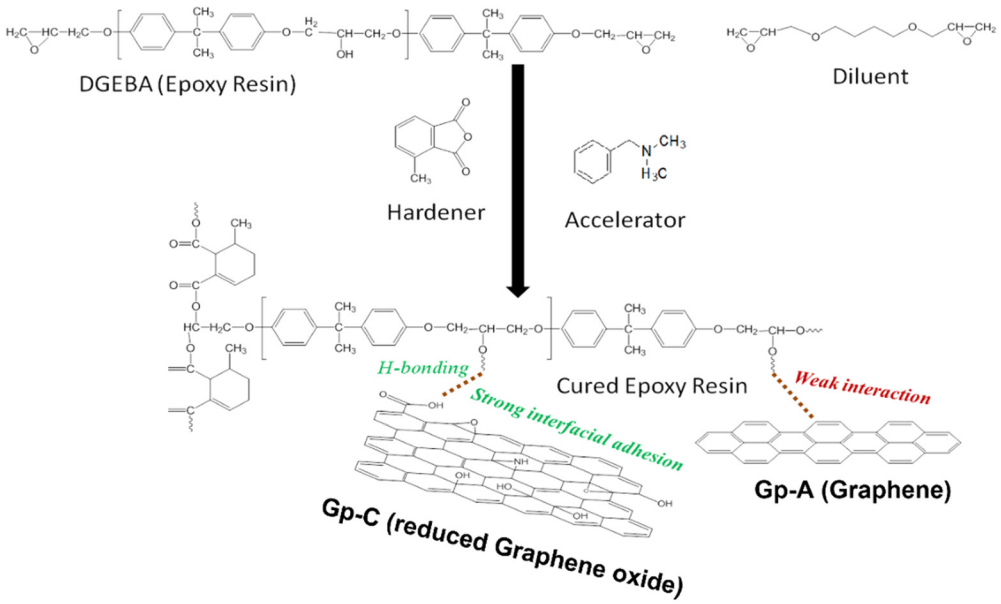

Fig. 5 Plausible and proposed mechanism for reinforcement in epoxy, functionalized (Gp-C), and non-functionalized (Gp-A) graphene composites.

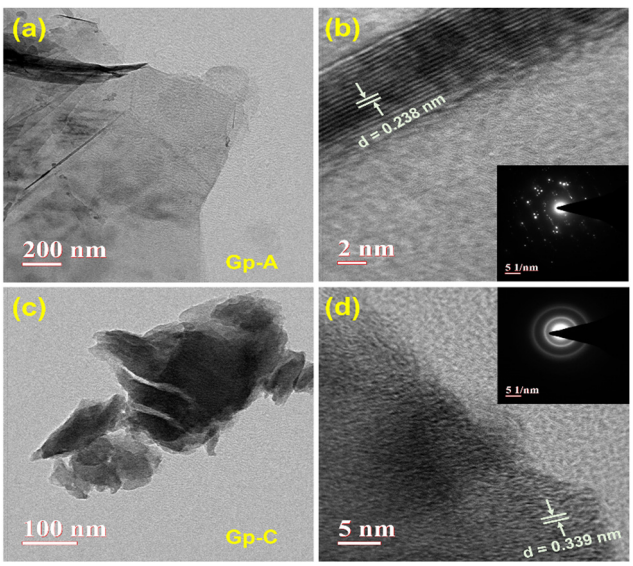

Fig. 6 HETEM micrographs of (a) and (b) epoxy/GNF composites; (c) and (d) epoxy/GF composites. The inset shows the SAED pattern with interlayer spacing of nano-additives.

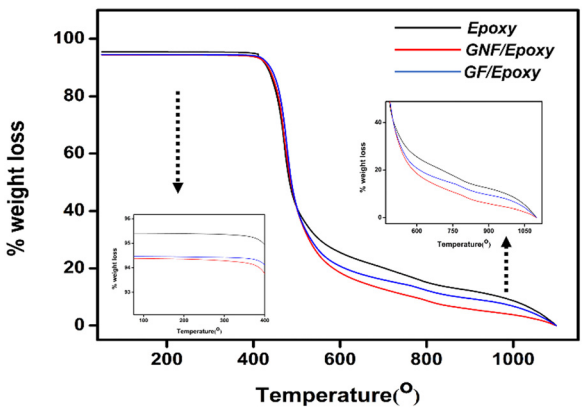

Fig. 7 Thermal gravimetric analysis of epoxy, and GF and GNF incorporated epoxy composites, through mechanical stirring.

investigate the influence of graphene on the composite's thermal stability, as depicted in Fig. 7. In the initial weight loss stage (<200 °C), a slight mass reduction is observed across all samples, primarily due to the evaporation of moisture and volatile compounds. The primary degradation phase (~350–500 °C) corresponds to the thermal breakdown of the epoxy matrix. Neat epoxy undergoes rapid decomposition in this range, whereas both GNF/epoxy and GF/epoxy show a shift toward higher degradation temperatures, confirming improved thermal resistance. The degradation follows a two-step mechanism: first (~330–430 °C), involving the breakdown of low-molecular-weight epoxy chains and primarily attributed to main chain pyrolysis,[42,43] and second (~430–500 °C), corresponding to the decomposition of the crosslinked polymer network. Pristine epoxy shows a 5% residue, but with the addition of 0.1 wt% graphene additives, the residue increases to 6% at 1100 °C, suggesting a minor enhancement in thermal stability. The weight loss percentage decreases as the temperature increases, which is attributed to improved interfacial interactions between the graphene (functionalized graphene exhibits more interaction compared to non-functionalized graphene)[44] and the epoxy matrix in the composites. At higher temperatures (600–1000 °C), the residual char content serves as an indicator of material stability under extreme conditions.

Next, we furthermore introduced glass fabric and coating with both GF and GNF/epoxy hardener systems for fabricating single-layer glass fiber laminates using hand lay-up at 0.5 mm

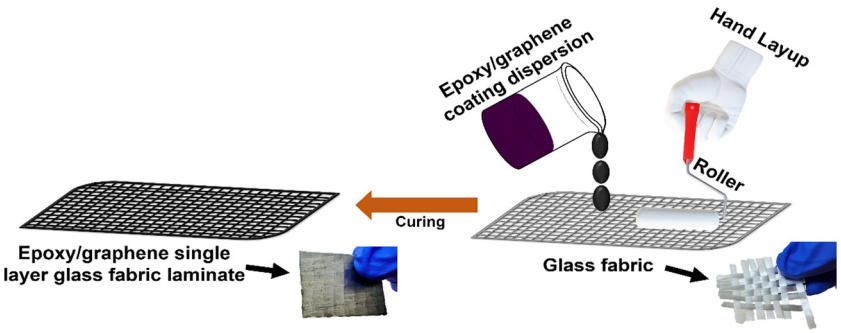

Fig. 8 Hand layup process for fabricating a single-layer glass fabric laminate composite based on epoxy/Gp-C & Gp-A.

coating thickness, illustrated in Fig. 8. The real-life applications include high mechanical tolerance and graphene reinforced fiber reinforced polymer (FRP) pipes along with the stable coating design for inner layer pipes. In the mechanical testing, the average tensile strength of the epoxy-SL laminates was around 345 ± 20 MPa, whereas GF/epoxy-SL having 420 ± 20 MPa, and GNF/epoxy-SL had 380 ± 20 MPa. In both cases, there was enhancement in strength, but GF shows better performance due to the functionalization and homogeneous dispersion within the epoxy matrix, which were also visualized in FESEM micrographs (Fig. 9).

In the antibacterial study, the prepared top-coated laminates were evaluated by measuring the zone of inhibition (ZOI) against *E. coli* (Gram-negative) and *S. aureus* (Gram-positive). Fig. 10 presents a digital image of various graphene-coated laminates alongside the reference single-layer epoxy laminates under agar plates, where the inhibition zones are clearly visible. The epoxy coating alone showed no inhibition zone, whereas the graphene-incorporated epoxy coatings (with 1 wt% graphene in the top layer) displayed ZOI values of 1.2 mm^2 for *E. coli* and 1.8 mm^2 for *S. aureus* in the GNF laminate and 0.8 mm^2 for both bacteria in the GF laminate. The sharp edges and surface characteristics of graphene can physically disrupt bacterial membranes,[45] cutting through the cell wall or inducing membrane stress, thereby enhancing its antibacterial

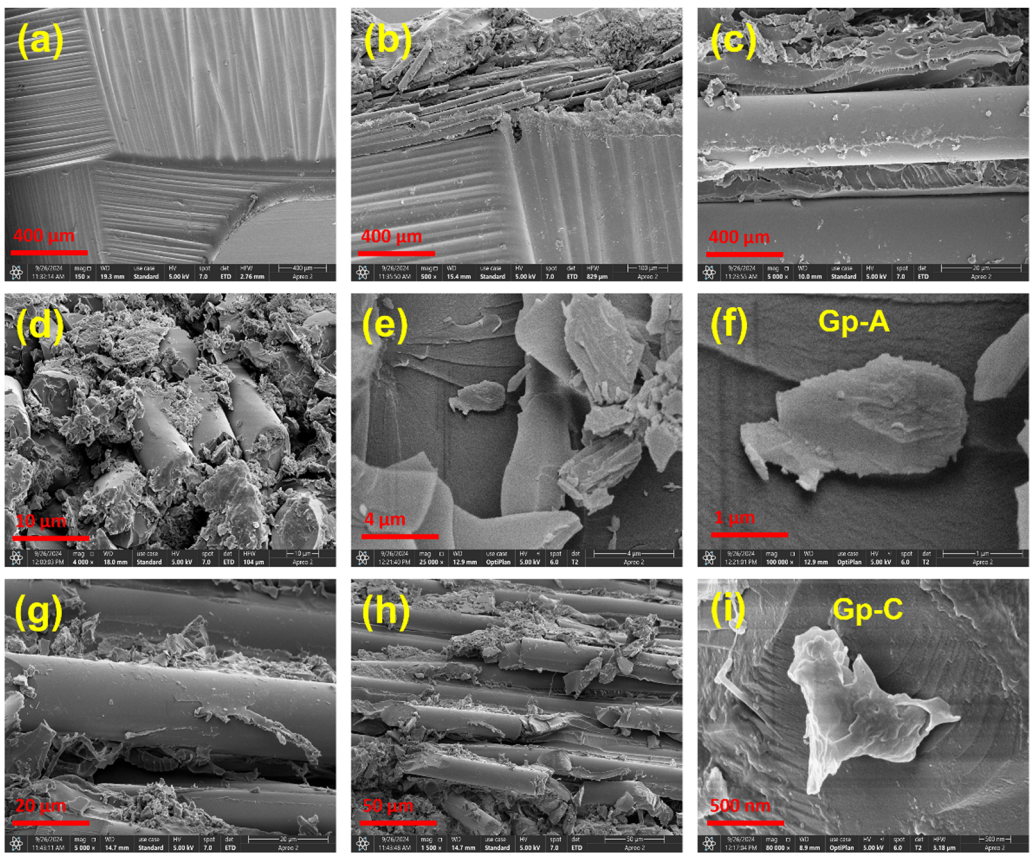

Fig. 9 FESEM micrographs of fractured (a)–(c) glass fabric/epoxy single layer laminates; (d)–(f) non-functionalized graphene/epoxy and (g)–(i) functionalized graphene/epoxy single layer laminates.

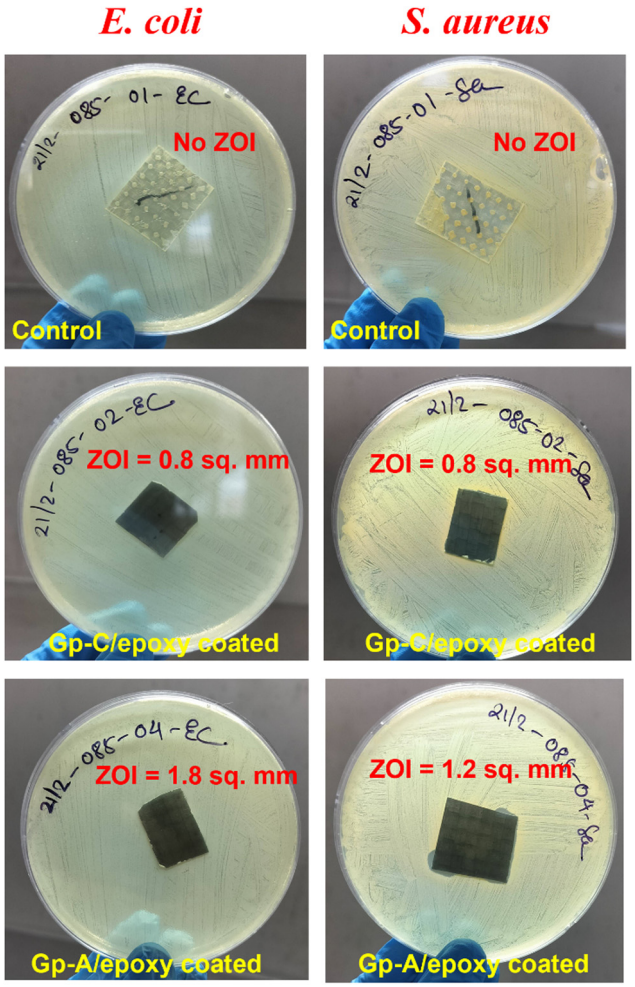

Fig. 10 Antibacterial features *via* ZOI measurements of top coating for *E. coli* and *S. aureus* bacteria.

effectiveness against both Gram-positive and Gram-negative bacteria. We expanded the analysis by performing colony-forming unit (CFU) testing following ISO 22196. This standard evaluates the antibacterial properties of non-porous surfaces by incubating bacteria, such as *E. coli* and *S. aureus*, on coated laminates and measuring their reduction after 24 hours. The antimicrobial efficacy is expressed as a log reduction value, making this a crucial test for assessing antimicrobial coatings and materials. The antibacterial efficacy of Gp-A/epoxy and Gp-C/epoxy coatings was evaluated against *E. coli* and *S. aureus* over a 24-hour contact period, with plain epoxy serving as the control, as shown in Table S1 (ESI†). For *E. coli*, the control sample exhibited a bacterial count of 4.05×10^1 CFU per ml (log value: 1.61). The Gp-A/epoxy-coated sample showed complete antibacterial activity, with bacterial counts below the detection limit (<1 CFU per ml) and a log reduction of ≥1.61, indicating strong antimicrobial performance. The Gp-C/epoxy-coated sample had a bacterial count of 3.00 CFU per ml (log value: 0.48), achieving a log reduction of 1.13, suggesting moderate antibacterial action. For *S. aureus*, the control sample exhibited a high bacterial count of 5.10×10^5 CFU per ml (log value: 5.71). The Gp-A/epoxy-coated sample reduced the bacterial count to 1.61×10^5 CFU per ml (log value: 5.21), achieving a log reduction of 0.49, indicating mild antibacterial activity. In contrast, the Gp-C/epoxy-coated sample demonstrated significant antibacterial efficacy, reducing the bacterial count to 2.15×10^2 CFU per ml (log value: 2.33), with a log reduction of 3.38, highlighting its strong antimicrobial properties. These findings indicate that while Gp-A/epoxy shows excellent antibacterial performance against *E. coli* and moderate effects against *S. aureus*, Gp-C/epoxy provides substantial antibacterial action against both bacteria, making it a more effective candidate for antimicrobial applications.

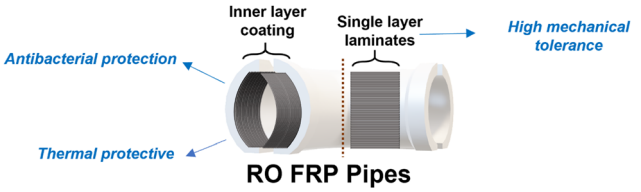

Fig. 11 Two-way approach for enhancement of durable fiber-reinforced polymer (FRP) RO pipes: (a) inner layer coating with epoxy/graphene, which enhances antibacterial and thermal protection, and (b) FRP pipes with incorporation of graphene/epoxy glass fabrics.

Finally, a two-way approach is proposed for enhancing the durability and performance of fiber-reinforced polymer (FRP) reverse osmosis (RO) pipes, illustrated in Fig. 11. The first strategy involves coating the inner layer of the pipes with an epoxy/graphene composite, providing enhanced antibacterial properties and improved thermal protection. This inner coating serves as a protective barrier, reducing biofouling and thermal degradation. The second approach incorporates graphene/epoxy glass fabrics within the FRP pipe structure, significantly increasing the mechanical strength and durability of the pipes. Together, these methods offer a robust solution for improving the longevity and efficiency of FRP RO pipes in demanding environments.

5. Conclusion

Epoxy resin continues to play a vital role in composite materials, offering a balance of mechanical strength, durability, and versatility. This current study aims to explore the state-of-the-art developments in epoxy resin-functionalized/non-functionalized graphene (industrial-based graphene additives *e.g.*, Gp-C as GF and Gp-A as GNF). Castings have been prepared *via* industrially feasible, both high-speed shearing and mechanical stirring processes (variation of both RPM and time of mixing). We have provided insights into the mechanisms of reinforcement and the resulting improvements in material properties along with a comparison study. Furthermore, we have extended the scope of this study by fabricating, single-layer glass fabric laminates with an epoxy/graphene system to develop high-performance fiber-reinforced polymer systems (FRPs). This approach led to notable improvements in mechanical properties, with increases of approximately 10% and 22%

through the incorporation of GNF and GF fillers, respectively. Additionally, we applied these systems to create stable coating solutions for top-coated FRPs, thereby providing effective antibacterial protection. The zones of inhibition (ZOI) are 1.2 mm^2 for *E. coli* and 1.8 mm^2 for *S. aureus* in the GNF laminate, and 0.8 mm^2 for both bacteria in the GF laminate, respectively. The antibacterial effectiveness of graphene/epoxy laminates was assessed through CFU (colony-forming unit) testing. It showed that GNF achieved a log reduction of ≥ 1.61 for *E. coli* and 0.49 for *S. aureus*, whereas GF exhibited improved antibacterial performance with log reductions of 1.13 for *E. coli* and 3.38 for *S. aureus*. This enhanced activity is linked to ROS-induced oxidative stress and disruption of the bacterial membrane. The results highlight the potential of the graphene/epoxy composites for water treatment (FRP pipes and filtration membranes), medical coating (devices and hospital surfaces), construction (FRP panels and antimicrobial flooring), aerospace and automotive (lightweight, heat-resistant materials), and marine (anticorrosion coatings) applications. Their durability, antibacterial properties, and thermal stability make them ideal for high-performance, long-lasting applications, with a future focus on scalability and sustainability.

Data availability

Data will be made available on request.

Conflicts of interest

There are no conflicts to declare.

Acknowledgements

The authors gratefully acknowledge the financial support provided by DCM Shriram Innovation Centre (DSIC) and DCM Shriram Ltd for carrying out this work. They also extend their appreciation to Tata Steel, India, for their technical support and guidance. SG wants to thank Mr Murlidhar Totla, Analytical Executive, DSIC, for helping with thermal characterization.

References

1 J. M. Sousa, J. R. Correia and S. Cabral-Fonseca, *Constr. Build. Mater.*, 2018, **161**, 618–633.
2 A. Rudawska, *Appl. Mech.*, 2021, **2**, 108–126.
3 P. K. Balguri, D. H. Samuel and U. Thumu, *Mater. Today: Proc.*, 2021, **44**, 346–355.
4 A. C. Garg and Y.-W. Mai, *Compos. Sci. Technol.*, 1988, **31**, 179–223.
5 S. Kumar, S. Krishnan, S. K. Samal, S. Mohanty and S. K. Nayak, *Ind. Eng. Chem. Res.*, 2018, **57**, 2711–2726.
6 S. Ghosh, B. Nitin, S. Remanan, Y. Bhattacharjee, A. Ghorai, T. Dey, T. K. Das and N. C. Das, *ACS Appl. Mater. Interfaces*, 2020, **12**, 17988–18001.
7 P. Feraboli, T. Cleveland, M. Ciccu, P. Stickler and L. DeOto, *Composites, Part A*, 2010, **41**, 888–901.
8 R. V. Patel, A. Yadav and J. Winczek, *Appl. Sci.*, 2023, **13**, 5126.
9 S. Ghosh, I. Greenfeld and H. D. Wagner, *Composites, Part A*, 2023, **167**, 107427.
10 D. W. Mulqueen, S. Sattar and O. G. Kravchenko, *Composites, Part B*, 2023, **255**, 110609.
11 M. M. Shariff, G. R. Arpitha, N. Jain, U. Shankar, A. Verma and N. D. Shivakumar, *Hybrid Adv.*, 2023, **4**, 100095.
12 G. R. Arpitha, N. Jain, A. Verma and M. Madhusudhan, *Biomass Convers. Biorefin.*, 2024, **14**(11), 12531–12538.
13 N. Ilie, K. Felten, K. Trixner, R. Hickel and K.-H. Kunzelmann, *Dent. Mater.*, 2005, **21**, 483–489.
14 X. Zhao, J. Pan, S. Zhang, H. S. Malmstrom and Y.-F. Ren, *Clin. Oral Investig.*, 2017, **21**, 463–468.
15 P. Cai, Y. Wang, T. Wang and Q. Wang, *Tribol. Int.*, 2015, **87**, 1–10.
16 M. Baig and M. A. Samad, *Polymers*, 2021, **13**, 179.
17 R. F. Gibson, *Compos. Struct.*, 2010, **92**, 2793–2810.
18 J. Viana, *Plast., Rubber Compos.*, 2006, **35**, 260–267.
19 G. Ahmetli, H. Deveci, U. Soydal, S. P. Gurler and A. Altun, *J. Appl. Polym. Sci.*, 2012, **125**, 38–45.
20 H. Ma, M. A. Aravand and B. G. Falzon, *Compos. Sci. Technol.*, 2022, **217**, 109095.
21 Z. Anwar, A. Kausar, I. Rafique and B. Muhammad, *Polym.-Plast. Technol. Eng.*, 2016, **55**, 643–662.
22 L.-J. Cui, Y.-B. Wang, W.-J. Xiu, W.-Y. Wang, L.-H. Xu, X.-B. Xu, Y. Meng, L.-Y. Li, J. Gao and L.-T. Chen, *Mater. Des.*, 2013, **49**, 279–284.
23 S.-J. Park and Y.-H. Kim, *Mod. Phys. Lett. B*, 2019, **33**, 1940051.
24 Z. Bouyahia, A. Mdarhri, A. Benayad, C. Brosseau, I. Elaboudi, D. Chicot, A. Iost, D. He and J. Bai, *J. Appl. Polym. Sci.*, 2021, **138**, 50697.
25 W. Kong, H. Kum, S.-H. Bae, J. Shim, H. Kim, L. Kong, Y. Meng, K. Wang, C. Kim and J. Kim, *Nat. Nanotechnol.*, 2019, **14**, 927–938.
26 A. K. Geim, *Science*, 2009, **324**, 1530–1534.
27 W. Du, X. Jiang and L. Zhu, *J. Mater. Chem. A*, 2013, **1**, 10592–10606.
28 M. Ioniță, G. M. Vlăsceanu, A. A. Watzlawek, S. I. Voicu, J. S. Burns and H. Iovu, *Composites, Part B*, 2017, **121**, 34–57.
29 A. N. Obaid and E. Al-Bermany, *Int. J. Adhes. Adhes.*, 2024, **132**, 103695.
30 A. N. Obaid and E. Al-Bermany, *Mater. Chem. Phys.*, 2023, **305**, 127849.
31 K. E. Awwad, B. Yousif, K. Fallahnezhad, K. Saleh and X. Zeng, *Friction*, 2021, **9**, 856–875.
32 Y. Li, R. Umer, A. Isakovic, Y. A. Samad, L. Zheng and K. Liao, *RSC Adv.*, 2013, **3**, 8849–8856.
33 A. Shrestha, Y. Sumiya, K. Okazawa, T. Uwabe and K. Yoshizawa, *Langmuir*, 2023, **39**, 5514–5526.
34 K. K. Singh, R. Prabhu B, S. Choudhary, C. Pramanik and N. S. John, *ACS Omega*, 2019, **4**, 14569–14578.
35 Y. Yang, G. Xian, H. Li and L. Sui, *Polym. Degrad. Stab.*, 2015, **118**, 111–119.

36 E. A. Awwad, B. F. Yousif, K. Fallahnezhad, K. Saleh and X. Zeng, *Friction*, 2021, **9**, 856–875.
37 M. M. Gudarzi and F. Sharif, *eXPRESS Polym. Lett.*, 2012, **6**(12), 1017–1031.
38 M. Goyat, A. Hooda, T. K. Gupta, K. Kumar, S. Halder, P. Ghosh and B. S. Dehiya, *Ceram. Int.*, 2021, **47**, 22316–22344.
39 S. K. Yadav and J. W. Cho, *Appl. Surf. Sci.*, 2013, **266**, 360–367.
40 J. Fan, J. Yang, L. Wang, H. Li, J. Tian, J. Ye and Y. Zhao, *Appl. Surf. Sci.*, 2021, **558**, 149964.
41 M. Lotya, Y. Hernandez, P. J. King, R. J. Smith, V. Nicolosi, L. S. Karlsson, F. M. Blighe, S. De, Z. Wang and I. McGovern, *J. Am. Chem. Soc.*, 2009, **131**, 3611–3620.
42 M. Luda, A. Balabanovich, M. Zanetti and D. Guaratto, *Polym. Degrad. Stab.*, 2007, **92**, 1088–1100.
43 E. Al-Bermany and B. Chen, *Macromol. Chem. Phys.*, 2023, **224**(16), 2300101.
44 E. Al-Bermany and R. Chen, *Polym. Int.*, 2021, **70**(3), 341–351.
45 S. Ghosh, S. Ganguly, P. Das, T. K. Das, M. Bose, N. K. Singha, A. K. Das and N. C. Das, *Fibers Polym.*, 2019, **20**, 1161–1171.